8-9-2006

Gold and Magnetite Nanoparticles as Sensors of Conformational Changes in Proteins

Larisa Radu
University of New Orleans

GOLD AND MAGNETITE NANOPARTICLES

AS SENSORS OF CONFORMATIONAL CHANGES IN PROTEINS

A Thesis

Submitted to the Graduate Faculty of the
University of New Orleans
in partial fulfillment of the
requirements for the degree of

Master of Science
in
Chemistry

by

Larisa Cristina Radu

B.S. "Gr. T. Popa" University of Medicine and Pharmacy, Iasi, Romania, 2003

August 2006

Acknowledgments

First, I would like to express my sincere gratitude to my research advisor Professor John B. Wiley, for help, advice and guidance throughout my graduate studies. I am grateful to Professor Paul Hanson, for guidance and invaluable encouragement throughout my graduate research. I would like to thank my committee member, Professor Jiye Fang, for useful discussions and constructive suggestions.

I would also like to thank Daniela Caruntu for providing the magnetite nanoparticles and for help in taking the electron microscopy images.

I am grateful to my colleagues in Dr.Wiley's group for their help and friendship.

Last but not least, my special thanks go to my parents to whom I owe everything.

Table of Contents

Abstract iv

Introduction 1

Chapter 1 Studies of Protein Folding using Gold Nanoparticles 5
- 1.1 Introduction 5
- 1.2 Experimental section 6
  - 1.2.1 Materials and equipment 6
  - 1.2.2 Preparation of the polypeptide 7
  - 1.2.3 Preparation of the polypeptide-Au nanoparticles bioconjugates 8
- 1.3 Results and discussion 9
  - 1.3.1 Characterization of polypeptide-Au nanoparticles bioconjugates using UV-Vis spectrophotometry 9
  - 1.3.2 Characterization of polypeptide-Au nanoparticles bioconjugates using TEM 11
  - 1.3.3 Discussion 12
- 1.4 Conclusions 15

Chapter 2 Studies of Protein Folding using Magnetite Nanoparticles 16
- 2.1 Introduction 16
- 2.2 Experimental section 18
  - 2.2.1 Materials and equipment 18
  - 2.2.2 Preparation of the magnetite nanoparticles 19
  - 2.2.3 Preparation of the ligands-magnetite nanopaticles bioconjugates 20
- 2.3 Results and discussion 20
  - 2.3.1 Characterization of magnetite nanoparticles in methanol solution using EPR spectroscopy 21
  - 2.3.2 Characterization of citric acid-magnetite nanoparticles bioconjugates using EPR spectroscopy 24
  - 2.3.3 Characterization of salts-magnetite nanoparticles bioconjugates using EPR spectroscopy 25
  - 2.3.4 Characterization of proteins-magnetite nanoparticles bioconjugates using EPR spectroscopy 26
  - 2.3.5 Characterization of magnetite nanoparticles in methanol solutions using EPR spectroscopy as a function of temperature 27
  - 2.3.6 Discussion 29
- 2.4 Conclusions 32

References 33

Vita 36

Abstract

The folding of proteins was investigated by using helical polypeptides attached to gold or magnetite nanoparticle surfaces.

Depending on type and loading of the polypeptide on the surface of gold nanoparticles, pH, temperature, presence of different ions in the solution, and influence of different mechanical factors, conformational changes in the polypeptide occurred. The aggregation of the gold nanoparticles related to the folding of the polypeptide caused shifts in color of the solutions from red to blue that were measured by UV-Vis spectrometry.

Different ligands were attached on the surface of magnetite nanoparticles. The resulting structures induced modifications in the characteristics of the superparamagnetic resonance (SRP) spectra of magnetite nanoparticles. Lineshape parameters related to the anisotropy and crystal structure revealed ligand-dependent and temperature-dependent SPR spectra. The attachment of ligands leads further to the possibility of attaching model polypeptides on the magnetite nanoparticles surface for studying protein folding.

Introduction

21st century science deals extensively with the highly emerging field of nanomaterials. Nanomaterials are structures with dimensions in the mesoscopic range (between 1 and 100 nm). Physics and electronics are building nanostructures by using conventional top-down techniques like lithography and etching [1]. By self-assembly and building up of blocks, nature serves a great model for nanotechnology. Thus, today's chemistry and materials science are using bottom-up approaches, the biggest problems in the building process being the induction of molecular self-organization and the functionalization of the resulting nanostructures [2].

Lately, the combination of nanomaterials and biological molecules proved to be attractive for new applications in electronics, genomics, and biomedical and bioanalytical areas [3]. The linkage is currently done by modifying the biological molecules with a chemical group that is reactive towards the nanomaterial surface [4]. Biological molecules can be either absorbed on the surface of the nanomaterial [5] or they can form electrostatic interactions with the oppositely charged nanostructures [6]. Still, the most desired binding is through chemical bonds [7]. Extensive studies have been done on functionalized gold and magnetic nanoparticles [8]. Bioconjugation of Au nanoparticles with oligonucleotide via thiol group [1] or immobilization of different drugs on the surface of magnetite nanoparticles [1] were reported. DNA-modified Au nanoparticles have been used for the detection of DNA-sequences [9]. Au nanoparticles proved also to be effective carriers for the delivery of DNA into the cell [1]. Cd/Se nanoparticles coated with biological ligands specific for certain cellular structures were used in fluorescence labeling of cells [10].

Drugs attached to the surface of magnetic nanoparticles were directed with magnetic fields to the target tissues [11]. Magnetic nanoparticles incorporated into malignant cells and excited with alternating magnetic fields were also used in order to increase local temperature that induced hyperthermia [12].

However, the attaching of proteins to the surface of metallic nanoparticles is currently a real challenge. Proteins are either hydrophobic or hydrophilic, they have either positive or negative charge and their structures are complicated comparing to DNA and RNA. Thus, although a specific interaction between the proteins and nanoparticles is desired, in practice, the nonspecific binding often occurs [13]. While much effort has gone into the development of a specific proteins-nanoparticles binding for sensors and actuators applications, only a few studies focused on the conformational changes that occur when a protein encounters a surface [14]. The final goals of these studies are to detect and to understand the proteins conformation and to measure the nanomaterial surface coverage [14].

By folding into specific three-dimensional shapes, proteins are able to perform their biological functions. The particular amino-acid sequence that gives the primary structure of a protein determines how the protein will fold into its native conformation. The folding process depends on the characteristics of the proteins environment (solvent, concentration of salts, temperature) and is mediated by electrostatic interactions (hydrogen bonds, van der Waals interactions) between amino acid R groups [15]. These interactions establish the formation of the alpha helices and beta sheets (secondary structure). Tertiary and quaternary structure formation involves covalent bonding between cysteine residues, directing the assembly of the subunits that are already folded.

Folding is a spontaneous process. The phenomenon is driven by van der Waals forces and entropic contributions to the Gibbs free energy. Moving the hydrophobic amino acids of the protein inwards and the hydrophilic ones outwards produces an increase in entropy necessary for overcoming the energy barrier that allows the protein to achieve its native folding [16]. The time scale of the process depends mostly on the protein; the slowest folding require minutes, primarily due to steric hindrances, while typical folding needs only milliseconds [17].

The current interest in the folding process comes from the fact that incorrectly folded proteins are responsible for prion related diseases such as Creutzfeldt-Jacob disease and Bovine spongiform encephalopathy (mad cow disease), as well as amyloid related diseases such as Alzheimer disease. It is believed that the aggregation of misfolded proteins into insoluble plaques are the cause of these diseases [18].

Currently, protein folding is studied by expensive and complicated techniques like computational prediction of the conformation, circular dichroism, IR spectroscopy, X-ray crystallography and NMR. All these methods investigate protein structure in solution or on a two-dimensional surface; folding studies using proteins attached to three-dimensional surfaces (like nanoparticles) are still in an initial phase. A series of questions rise from these studies: are the proteins denatured or active, folded or unfolded, or how the proteins adsorption on the surface of the nanoparticles be controlled?

The hypothesis of our study is that the folding of a protein attached to a three-dimensional surface is basically identical to the one that occurs on a two-dimensional surface. This is the reason why we assumed that model polypeptides attached to either gold or magnetite nanoparticles surface can be used to investigate the folding and

unfolding of proteins. Because more than 50% of the natural proteins have helical structures and helices are the first structures that form in the folding process [16], we believe that a relatively short, helical polypeptide can serve as a simplified model for the study of a protein folding. Our resulting bio-nanostructures were investigated by transmission electron microscopy (TEM). A UV-Vis spectrophotometer was used to characterize the polypeptide-Au nanoparticles samples. An EPR spectrometer was used to characterize the ligands-magnetite nanoparticles.

Chapter 1

Studies of Protein Folding using Gold Nanoparticles

1.1 Introduction

Gold colloids are stable dispersions of Au nanoparticles in a liquid phase. The stability of the colloid is given by the structure of the Au nanoparticles: elemental gold core surrounded by two charged layers (a negative inner layer formed by $AuCl^-$ ions, called zeta potential, and a positive outer layer formed by H^+ ions) [19].

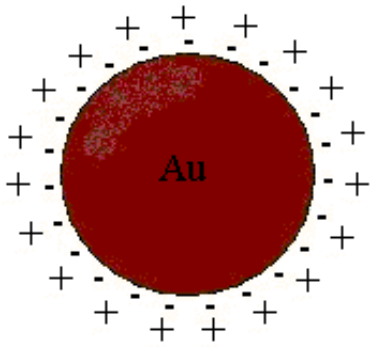

Figure 1.1: Gold nanoparticle surrounded by charged layers

Thiol groups bind covalently to the Au nanoparticles surfaces. Thus, for the bioconjugation of Au nanoparticles with proteins, it is easy to just add thiol-modified proteins to a solution of Au nanoparticles [4]. Thiol modified-proteins have cysteine residues accessible for interphase coupling and incorporated into their structure by chemical or genetic engineering methods [1].

The subsequent problems like the flocculation of colloidal gold by the protein and the failure of the protein to be absorbed by colloidal gold, can be solved through the application of concentration and pH variable adsorption isotherms [20,21].

Zare and collaborators proved that conformational changes in proteins can be studied using cytochrome C protein covalently attached to the surface of gold nanoparticles via a thiol bond [22]. The binding of the proteins to the surface of gold nanoparticles and the aggregation of the coated nanoparticles changed the color of the investigated solutions. The result was assumed to be a surface plasmon effect. Surface plasmon resonance is a quantum optical-electrical phenomenon that is produced by the interaction of light with a metal surface. Under certain conditions (only at a specific resonance wavelength), the energy carried by photons of light is transferred to packets of electrons (called plasmons) on a metal's surface [23] and the energy that is lost can be detected in the form of ultraviolet or visible radiation [24]. Although the change in color of the solutions in this study was due to the aggregation of the nanoparticles and not to the conformational changes in the protein, it is believed that these two phenomena are related [22].

1.2 Experimental section

1.2.1 Materials and equipment

Au nanoparticles with diameters of 5 nm, and respectively 10 nm, produced by modified tannic acid / citrate method that makes use of the tetrachloric acid ($HAuCl_4$) reduction [25], were purchased from Sigma-Aldrich. FmocAla, FmocLys and FmocCys amino acids were used for the synthesis of the model polypeptide. Organic solvents and the other chemicals of AR grade were used as received.

The model polypeptide was synthesized by using Fmoc procedure on an APEX peptide synthesizer [26]. HPLC Beckam-Coulter System Gold with a semiprep column at

220 nm was used to purify the resulting polypeptide. TEM images were taken on a JEOL Model 2010 electron microscope operated at 120 kV. A UV-Vis spectrophotometer was used to characterize the samples with respect to their wavelength and absorbance. The wavelength range used was between 500 and 700 nm since previous experiments showed that gold nanoparticles absorb at around 515 nm while polypeptide coated gold nanoparticles absorb at around 570 nm.

1.2.2 Preparation of the polypeptide

For studying the folding process, a helical polypeptide having the following sequence $AcAAAAKAAAAKAAAAKCNH_2$ (called 3K16) was synthesized based on Fmoc method [26]. The polypeptide chain was constructed on an insoluble solid Wang resin using dimethyl formamide (DMF) as a solvent. Piperdine diluted in DMF was used in order to remove the protective Fmoc group of the amino acids. The coupling step, in which the amide bond is formed, used HBTU (2-(1-benzotriazole-1-yl)-1,1,3,3-tetramethyluronium hexafluorophosphate) and HoBt (1-Hydroxybenzotriazole) in DMF (0.5 M) as coupling reagents. The polypeptide product was cleaved from the resin with a mixture of trifluoroacetic acid (TFA), ethane dithiol, distilled water and triisopropylsylane (TIS) in a proportion of 94/2.5/2.5/1% v/v. The purification of the crude polypeptide based on size and polarity was done by reverse phase liquid chromatography using HPLC with a semiprep column with packing material composed of silica particles. Typical water/acetonitrile HPLC solvents (99.9% HPLC grade water; 0.1% trifluoro acetic acid and 99.9% HPLC grade acetonitrile; 0.1% trifluoroacetic acid) and different methods [27] optimized to obtain better resolution of the peaks and shorter elution time were used for the purification of the resulting peptide.

In the figure below, the HPLC spectrum of the 3K16 polypeptide at 220 nm shows the peak produced by the polypeptide bond at a retention time of 16.417 minutes. The mass of the polypeptide was also confirmed by mass spectrometry at LSU Health Sciences Center.

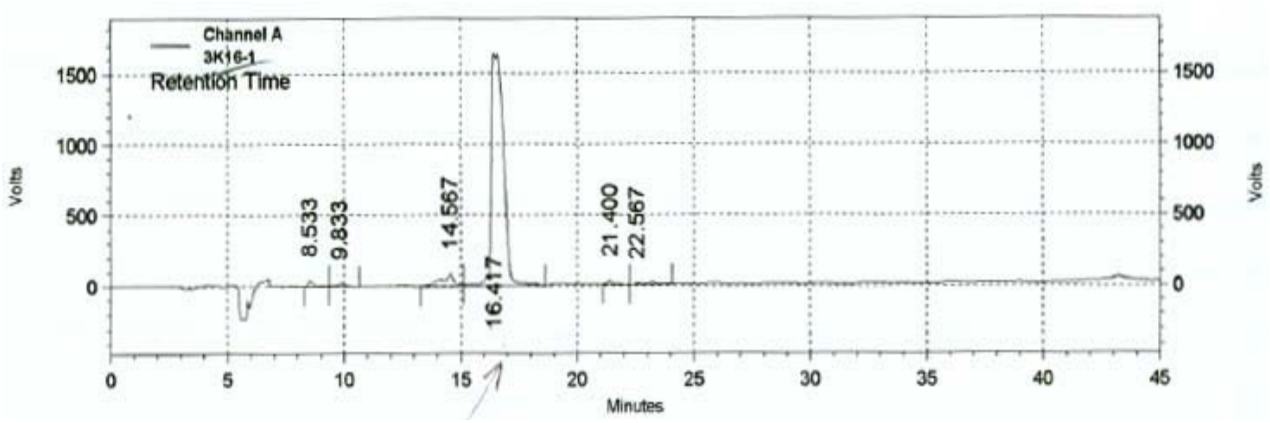

Figure 1.2: HPLC spectrum of 3K16 polypeptide

1.2.3 Preparation of polypeptide-Au nanoparticles bioconjugates

3K16 polypeptide is monomeric in solution and it has a temperature dependent helical content. To allow the binding to the surface of the gold nanoparticles via a thiol bond, a cysteine amino acid was incorporated at the C terminus of the polypeptide. The amino-acids sequence of 3K16 polypeptide was modified by attachment of an acetyl group at the N terminus (acetylation) and of a NH_3 group at the C terminus (amidation). Acetylation and amidation minimize unfavorable dipole-electrostatic interactions that would disrupt the helical folding of the polypeptide.

Starting with a concentrated $5*10^{15}$ molecules/μL stock 3K16 solution (0.83 mM), samples with ratios 6000:1, 1500:1, 750:1 and 600:1 polypeptide to Au nanoparticles (10 nm and respectively 5 nm) were prepared and their pH was measured as being 5.5 similar

to the gold colloid solution [25]. The resulting polypeptide-Au nanoparticles solutions were successively heated in a heat block 10 min at a temperature of 95^{o}C, cooled in ice 10 minutes and sonicated in a sonicator bath 1 minute. After each step the color of the solutions was visually observed, and the wavelength and the absorbance were measured by using a UV-Vis spectrophotometer.

1.3 Results and discussion

1.3.1 Characterization of polypeptide-Au nanoparticles bioconjugates using UV-Vis spectrophotometry

Depending on the loading of the polypeptide on the surface of gold nanoparticles, pH, temperature, or mechanical factors like sonication, particles aggregation was observed in the solutions. The wavelength and the absorbance were measured for these polypeptide-Au nanoparticles bioconjugates solutions before and after the appearance of the aggregation phenomenon, respectively before and after the sonication. The very broad peaks of UV-Vis spectrum obtained for each solution showed that aggregation of the nanoparticles occurred. Certain values for the maximum wavelength (λ) and the maximum absorbance (A) for the polypeptide-10 nm Au nanoparticles bioconjugates were measured initially; after 45 minutes and respectively after 2:30 hours, when the aggregate was settled, the wavelength and the absorbance of the solutions were measured again. A small shift in λ and an appreciable decrease in absorbance were observed. In contrast, when the samples were sonicated 1 minute, the wavelengths were almost equal to the initial measured wavelengths while the absorbencies were higher. For 5 nm nanoparticles the observations were similar, the λ shifts and the differences in absorbance

as a function of time and after sonication, being very small. Reproducing the procedure and measuring again the wavelength and the absorbance verified all these results. The values of wavelength and absorbance for 10 and 5 nm at ratios 600:1, 750:1 and 1500:1 polypeptide to nanoparticles are shown in the table below.

3K16/10 nm Au	**Solution + aggregate**		**Solution (after 45 min settling)**		**Solution (after 2:30 h settling)**		**Solution (after 1 min sonication)**	
ratio	*λ(nm)*	*A*	*λ(nm)*	*A*	*λ(nm)*	*A*	*λ(nm)*	*A*
600:1	576	0.346	566	0.128	594	0.087	567	0.162
750:1	580	0.552	580	0.379	583	0.309	582	0.395
1500:1	567	0.229	570	0.079	600	0.057	567	0.113
3K16/5 nm Au	**Solution + aggregate**		**Solution (after 45 min settling)**		**Solution (after 2:30 h settling)**		**Solution (after 1 min sonication)**	
ratio	*λ(nm)*	*A*	*λ(nm)*	*A*	*λ(nm)*	*A*	*λ(nm)*	*A*
600:1	535	0.856	535	0.853	534	0.841	533	0.787
750:1	560	0.794	559	0.702	558	0.692	556	0.720
1500:1	541	0.626	541	0.459	537	0.350	538	0.502

Table 1.1: Wavelength and absorbance at different polypeptide to Au nanoparticles (10 nm and 5 nm) ratios as a function of time and sonication

To test the influence of the temperature on the polypeptide-Au nanoparticles bioconjugates behavior in solutions, 600:1, 750:1, 1500:1 and 6000:1 3K16 polypeptide to Au nanoparticles (10 and 5 nm) ratios were investigated before and after thermic treatments. The samples were successively cooled in ice 1 hour, heated at 95^{o}C 10 minutes, cooled again 10 minutes, and finally, sonicated 1 minute. λ and A were measured after each step and their values are shown below.

3K16/ 10 nm Au	**initial**		**after 1h in ice**		**after 10min at 95^{o}C**		**after 10min in ice**		**after 1min sonication**	
ratio	*λ(nm)*	*A*	*λ(nm)*	*A*	*λ(nm)*	*A*	*λ(nm)*	*A*	*λ(nm)*	*A*
600:1	519	0.808	519	0.798	517	0.801	518	0.784	518	0.727
750:1	522	0.812	521	0.807	520	0.799	519	0.803	521	0.782
1500:1	519	0.815	519	0.810	517	0.809	517	0.812	519	0.738
3000:1	*524*	*0.837*	*524*	*0.787*	*520*	*0.782*	*520*	*0.762*	*521*	*0.773*
4000:1	*572*	*0.756*	*571*	*0.627*	*542*	*0.566*	*543*	*0.590*	*537*	*0.726*
6000:1	570	0.831	567	0.374	538	0.463	556	0.980	533	0.887

3K16/ 5 nm Au	initial		after 1h in ice		after 10min at 95°C		after 10min in ice		after 1min sonication	
ratio	*λ(nm)*	*A*	*λ(nm)*	*A*	*λ(nm)*	*A*	*λ(nm)*	*A*	*λ(nm)*	*A*
600:1	516	0.751	516	0.747	515	0.771	514	0.769	515	0.745
750:1	518	0.768	518	0.775	516	0.774	515	0.780	517	0.762
1500:1	524	0.783	524	0.824	522	0.832	522	0.833	521	0.793
6000:1	533	0.857	530	0.810	523	0.784	521	0.779	521	0.697

Table 1.2: Wavelength and absorbance at different polypeptide to Au nanoparticles (10 nm and 5 nm) ratios as a function of temperature and sonication

1.3.2 Characterization of polypeptide-Au nanoparticles bioconjugates using TEM

TEM observation for two samples 3K16-10 nm Au nanoparticles with 6000 : 1 ratio was performed. TEM images taken immediately after the sample preparation (mixing of 3K16 and 10 nm Au nanoparticles) revealed dispersed and aggregated Au nanoparticles, and organic material as well (Figure 1.3). The sample examined after overnight full saturation showed the existence of only aggregated nanoparticles (Figure 1.4).

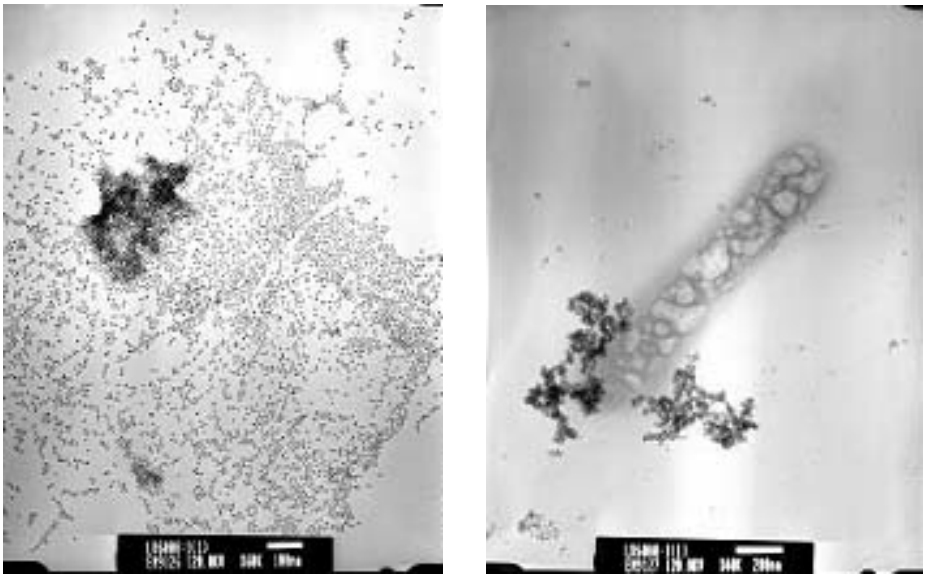

Figure 1.3: TEM images of 6000:1 ratio 3K16-10 nm Au nanoparticles sample immediately after preparation

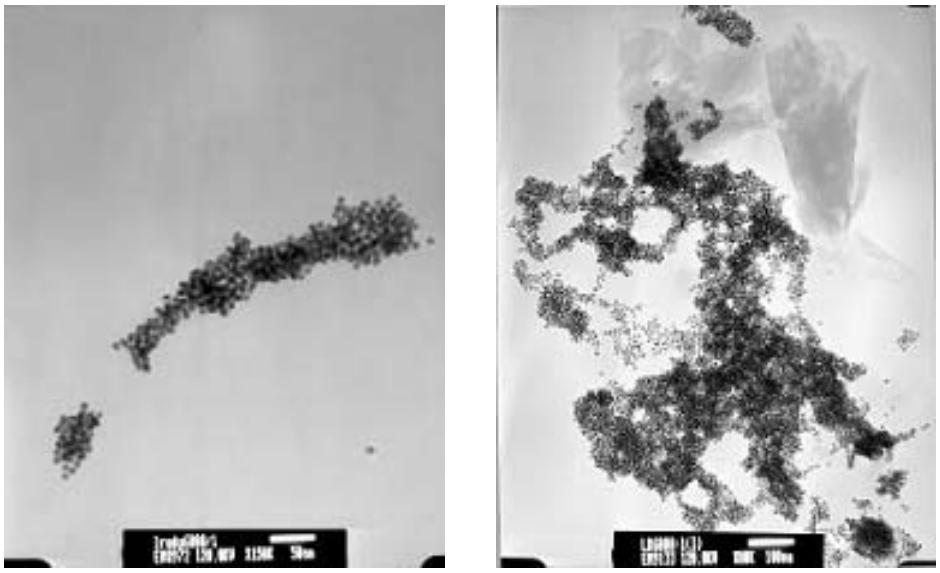

Figure 1.4: TEM images of 6000:1 ratio 3K16-10 nm Au nanoparticles sample after overnight full saturation

1.3.3 Discussion

The change in color from red (in the Au nanoparticles stock solution) to pink (the initial color of the 3K16 polypeptide-Au nanoparticles solutions with 6000:1 and 1500:1 ratios) and then to blue (in the same samples) is an indicator of the increase in size of the nanoparticles due to the bioconjugation that has been established between the nanoparticles surface and the polypeptide. This phenomenon is the result of the specificity of the thiol bond present in the cysteine terminal amino acid of the 3K16 polypeptide for the Au surfaces. The change in color is also the result of the aggregation of coated nanoparticles that might be caused by the hydrophobic interactions established between the polypeptide molecules covalently bound on the surface of Au nanoparticles.

The experiments also showed that temperature is an important factor in the process of polypeptide folding. At lower temperatures, the polypeptide is more folded and

the solutions are colored. At high temperatures, the polypeptide is less folded with lighter colors or even almost clears solutions. These color changes are quantified by the variations in measured wavelengths and absorbencies. In case of 3K16-10 nm Au nanoparticles with small ratios 600:1, 750:1, and 1500:1, the shifts in wavelengths and the differences in absorbencies are almost imperceptible. For the same nanoparticle diameter, 6000:1 ratio solution that was cooled in ice 1 hour, the increase in the wavelength indicates that the polypeptide is folded between λ = 556-567 nm. The data also showed that the polypeptide is unfolded when heated at 95 ^{o}C at λ = 538 nm and after 1 minute sonication at λ = 533 nm. Unfolding takes place due to the hydrophobic interactions that prevent proper helical conformation of the polypeptide [16]. The 3K16-10 nm Au nanoparticles, 3000:1 ratio sample has a similar behavior as the smaller polypeptide to nanoparticles ratios (600:1, 750:1 and 1500:1), while the 4000:1 ratio behavior resembles to the 6000:1 one. The conformational changes in the polypeptide seem to be easily detected at ratios higher than 4000:1, 3K16 polypeptide to Au nanoparticles. In conclusion, variation in temperature affects the protein folding and unfolding, so it can affect the aggregation process of the polypeptide coated Au nanoparticles in solutions.

For 3K16 polypeptide-5 nm Au nanoparticles samples, the similar values of λ and A from one experiment to another prove that the solutions color did not change as a function of temperature. Because there are around 5000 Au atoms on the surface of each 5 nm Au nanoparticle (comparing with around 10000 Au atoms on the surface of each 10 nm Au nanoparticle), it means that on a 5 nm Au nanoparticle surface there are more polypeptide molecules than Au atoms, so the interactions that establish between the

polypeptides on the surface of the nanoparticles seem to be responsible for the particular behavior of the 3K16-5 nm Au nanoparticles solutions.

Sonication may also prevent the correct folding and as a result, the misfolding of the polypeptide may occur. Although because of the aggregation disappearance, our first hypothesis was that the polypeptide molecules are removed from the surface of the Au nanoparticles in the sonicated samples, the final observation of the aggregation after 24 hours showed that the polypeptide is still on the surface of the nanoparticles. The disappearance of the aggregate and the color change from purple to clear are due to a conformational change in the polypeptide (maybe to the misfolding of the polypeptide that is responsible for the aggregation of the nanoparticles after the sonication of the solutions).

At higher ratios 3K16-Au nanoparticles (1500:1 and 6000:1) for both nanoparticles diameters (5 and 10 nm), the hydrophobic interactions between the polypeptides are stronger than the electrostatic interactions that keep the nanoparticles dispersed in the solution and this is the reason why aggregation and change in color occur. At small ratios 3K16-Au nanoparticles (750:1 and 600:1) for both nanoparticles diameters (5 and 10 nm), the electrostatic forces are stronger than the hydrophobic ones and the solutions are stable. The experiments showed that the stability of the polypeptide-Au nanoparticles solutions used for studying the folding process is governed by the polypeptide load on the surface of the Au nanoparticles, and also by the pH and temperature of the solutions. The results can be used in order to construct binding isotherms specific for the 3K16 helical model polypeptide.

1.4 Conclusions

3K16 helical polypeptide is a proper model that mimics the behavior of a helical protein, so the method can be extended to the study of the protein folding. Although the quantified color changes in the solutions are the result of the aggregation of the polypeptide coated Au nanoparticles, the aggregation is directly related to the changes in the conformation of the attached polypeptide. Thus, Au nanoparticles can be used to create a colorimetric sensor for proteins conformational changes.

Chapter 2
Studies of Protein Folding using Magnetite Nanoparticles

2.1 Introduction

Iron oxide nanoparticles are highly attractive to biological and medical applications due to their magnetic properties, chemical stability and biocompatibility. Although magnetite nanoparticles are known as magnetic contrast agents [28] and drug delivery vehicles [29], to our knowledge, magnetite nanoparticles have not been used before for the study of protein folding.

Enhanced details of the magnetic characteristics of magnetite nanoparticles come from superparamagnetic (SPR) resonance studies. SPR is the resonant absorption of microwave radiation by superparamagnetic ions or molecules, with unpaired electron spins, in the presence of a static magnetic field [30]. SPR provides information about nanoparticles size, concentration, their magnetic anisotropy and coordination environment [31] and unlike electron paramagnetic resonance (EPR), it investigates systems containing many unpaired electrons. The SPR spectra of different superparamagnetic systems are characterized by the existence of a single line of a hyperlorentzian form close to the effective *g*-factor value $g_{eff} = 2.0$ [31]. Nanoparticles size-distribution and shape, their concentration, chemical environment, and not lastly, the temperature, are factors that influence the line-shape of the SPR spectrum. The temperature dependence of the linewidth is considered to be the consequence of the thermal fluctuations of the nanoparticles magnetic moments orientation with respect to the orientation of the applied magnetic field [32].

Three parameters are used to characterize SPR spectra: the polycrystalline effective *g*-factor, g_{eff}, the linewidth, ΔB, and the asymmetry ratio, A [33].

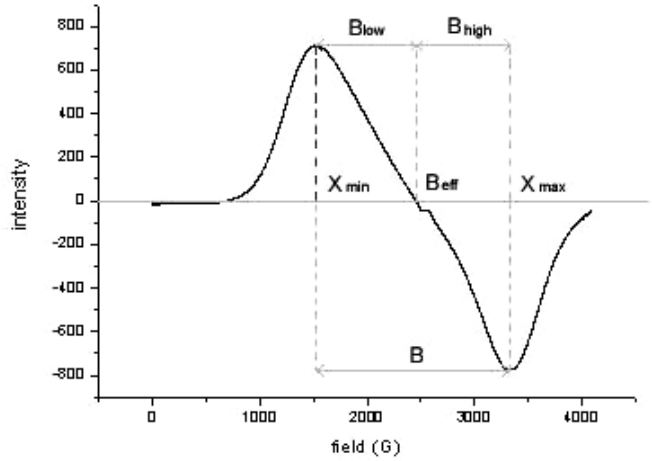

Figure 2.1: Parameters of the SPR spectra

The true *g*-factor is defined as:

$$g = \frac{h\nu}{\beta B_{rfe}}$$, where h is the Planck's constant, ν is the X-band microwave frequency, β is the Bohr magneton, and B_{rfe} is the applied field at which the maximum absorption occurs when the samples have no magnetic anisotropy [34]. For samples with magnetic anisotropy, an effective *g*-factor is defined as:

$$g_{eff} = \frac{h\nu}{\beta B_{eff}} \quad .$$

The relation between the true g-factor and effective g-factor gives information about the magnetic anisotropy and the size of the magnetic nanoparticles.

The linewidth of the SPR spectrum, ΔB, is the distance between the maximum positive and negative peaks. The asymmetry ratio, A, is defined as the ratio between ΔB_{high} and ΔB_{low}, where ΔB_{high} and ΔB_{low} are half linewidths at half maximum on the integrated spectrum [34] (Figure 2.1).

By measuring the effective *g*-factor, g_{eff}, the linewidth, ΔB, and the asymmetry ratio, A, properties of the magnetic nanoparticles like magnetic anisotropy, nanoparticle size, composition and concentration, can be precisely quantified. The existence of the different ligands on the magnetite particle surface can also be detected.

2.2 Experimental section

2.2.1 Materials and equipment

Magnetite nanoparticles with diameters of 10-12 nm in methanol were provided and used for our studies.

Acids (citric acid), salts (sodium carbonate, sodium acetate) and proteins (bovine serum albumin, BSA) were purchased from Sigma-Aldrich and used as ligands attached to the surface of the magnetite nanoparticles.

EPR experiments were performed on a Bruker EMX spectrometer equipped with a TE_{102} cavity, goniometer and variable temperature option. Samples of magnetite nanoparticles in different solvents, with or without ligands, were transferred to 100 μL quartz capillary tubes, and then flame-sealed. The X-band data (at a frequency of 9.8 GHz) were acquired at a power of 2-6 mW and a spectral width of 8000 Gauss with centerfield at 4000 Gauss. The modulation amplitude used was 10 Gauss, significantly less than the smallest linewidth. The time constant was 41 ms, the conversion time was 81.6 ms, and the frequency modulation was 100 kHz. For every experiment, the first-derivative of the absorption was monitored as a function of the applied field (B).

At the zero-crossing point in the first-derivative spectrum, the derivative of the power is zero ($dAbs/dB = 0$) and defines the resonance field (B_{eff}). The temperature dependence of the magnetic properties for the magnetite nanoparticles was studied from 100-370 K with increments of 10 K and accuracy of +/-0.1 K.

2.2.2 Preparation of the magnetite nanoparticles

Magnetite nanoparticles result from the hydrolysis of chelated alkoxide complexes of Fe^{2+} and Fe^{3+} in solutions of diethylene glycol (DEG) and N-methyl diethanol amine (NMDEA) and of diethylene glycol (DEG) and diethanol amine (DEA) at high temperature [35]. Magnetite, Fe_3O_4, has an inverse spinel crystal structure (Figure 2.2), $FeO \bullet Fe_2O_3$, with face centered cubic unit cell that contains 56 atoms: 32 O^{2-} anions, 16 Fe^{3+} cations (half of them tetrahedrally coordinated and the other half octahedrally coordinated) and 8 Fe^{2+} cations (all of them octahedrally coordinated) [36].

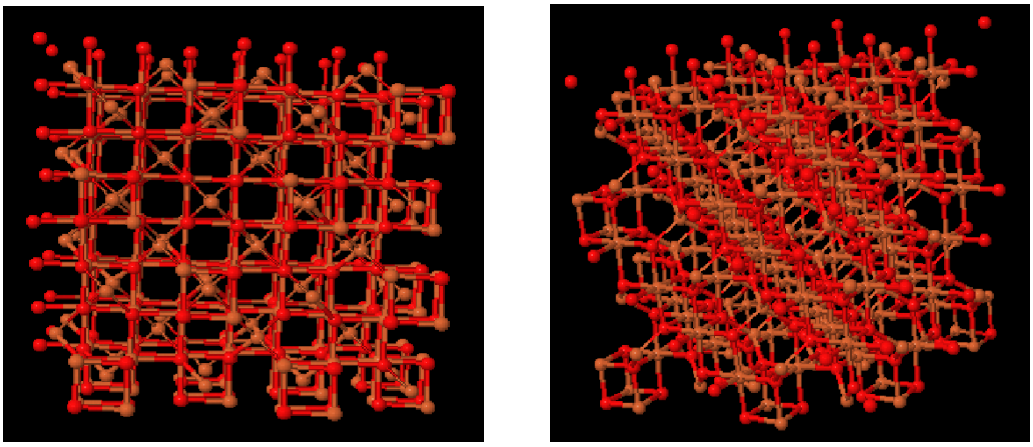

Figure 2.2: Magnetite, Fe_3O_4, inverse spinel crystal structure $FeO \bullet Fe_2O_3$

The synthesis of the magnetite is problematic because magnetite readily oxidizes in air to maghemite γ-Fe_2O_3, which is the reason why argon or nitrogen atmosphere is commonly used. Two different magnetite nanoparticles samples with diameters of 10-12

nm (with DEG and NMDEA on the surface, and respectively with DEG and DEA on the surface) were synthesized. The resulting magnetite nanoparticles were stored and provided to us in methanol after extensive washing in order to remove the chelating agents.

2.2.3 Preparation of the ligands-magnetite nanoparticles biocojugates

The EPR measurements were made for magnetite nanoparticles either in methanol or in methanol solutions with ligands. The transfer of the nanoparticles into the methanol-ligand solutions was accomplished first by isolating the magnetite nanoparticles with a strong magnet (5 Oe), washing them three times, and finally re-suspending them in the desired ligand-methanol solution. In cases when, under the influence of ligands, the nanoparticles precipitated, the solution was vortexed immediately prior to transfer into a quartz capillary tube. Dilutions (1:20, 1:40, 1:200, 1:1000) of magnetite in methanol, solutions of 9:1 magnetite nanoparticles to citric acid in methanol (0.25 mg/mL, 0.5 mg/mL, 1 mg/mL, 1.25 mg/mL, 1.5 mg/mL) and solutions of Fe_3O_4 nanoparticles in methanol (1 mg/mL) and cosolutes like sodium carbonate, sodium acetate and respectively bovine serum albumin (BSA) were prepared and used in the EPR studies.

2.3 Results and discussion

In magnetite, half of the 16 Fe^{3+} cations are tetrahedrally coordinated and the other half octahedrally coordinated, while all 8 Fe^{2+} cations are octahedrally coordinated by oxygen [36]. The distribution of Fe^{3+} and Fe^{2+} ions in octrahedral and tedrahedral sites is illustrated in the figure below.

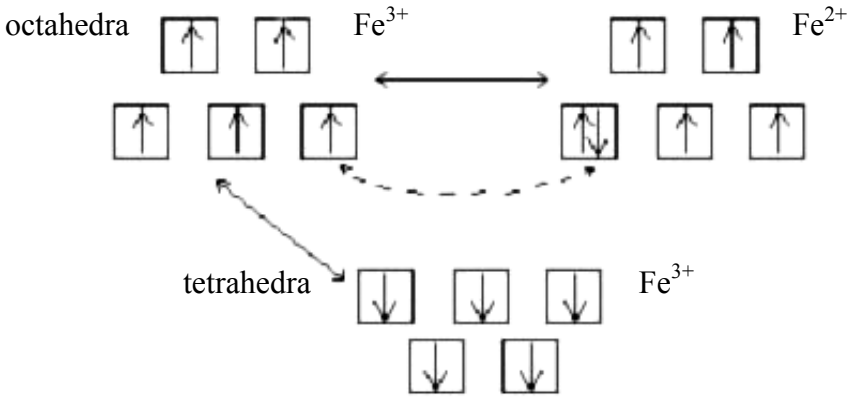

Figure 2.3: Magnetic behavior of magnetite, Fe_3O_4, ferromagnetic and antiferromagnetic couplings

The electron transfer from a high-spin Fe^{2+} to a neighboring Fe^{3+}, in octahedral sites, known as double exchange, favors the ferromagnetic ordering of the magnetic moments. Superexchange leads to an antiferromagnetic alignment of the spins on the tetrahedral iron and limits the magnetic behavior of the particles to $Fe^{3+} \leftrightarrow Fe^{2+}$ ferromagnetic coupling [37], which is detected by the EPR. Due to the electron migration between Fe^{3+} and Fe^{2+} ions, the real charge of the iron ions in magnetite is in fact, $Fe^{2.5+}$. Thus, Fe_3O_4 is ferrimagnetic.

2.3.1 Characterization of magnetite nanoparticles in methanol solutions using EPR spectroscopy

EPR spectrum for the magnetite nanoparticles in methanol sample (20 mg/mL) was acquired and used for comparison with all the other acquired spectra (Figure 2.4). Inter-particle dipolar exchange was demonstrated by the calculated parameters that characterize the EPR spectra (Table 2.1).

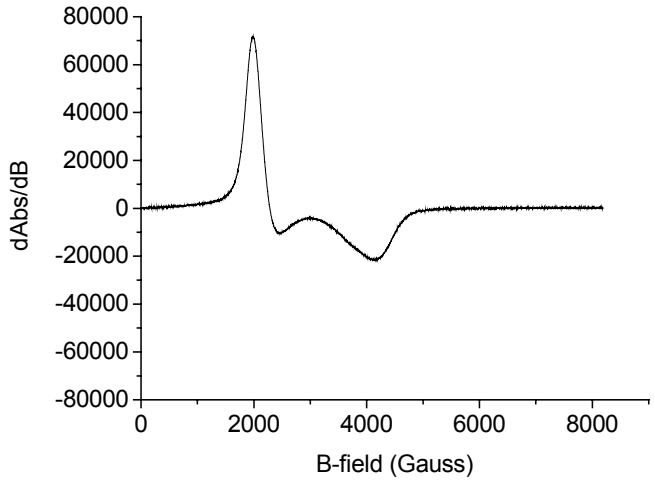

Figure 2.4: EPR spectrum of magnetite nanoparticles

sample	X_{min}	X_{max}	ΔB	B_{eff}	ΔB_{low}	ΔB_{high}	A	g_{eff}
Fe_3O_4	1982.36	4138.95	2156.59	2280.49	298.13	1858.46	6.23	3.1

Table 2.1: Parameters of magnetite nanoparticles EPR spectrum

Using magnetically dilute samples can minimize dipolar exchange effects. In order to find out the threshold concentration for which there is no spin-spin interactions between the nanoparticles, dilutions of magnetite samples in methanol were prepared. The EPR measurements are affected by variables like temperature and polarity [38]. Our experiments were done at room temperature but the difference in the spectra comes from the polarity of the solutions. Initial experiments done for different dilutions (1:20, 1:40, 1:200, 1:1000) of magnetite (both samples) in methanol showed that the magnetite EPR spectra vary with the polarity of the environment; the more polar the environment is, the broader the peaks are.

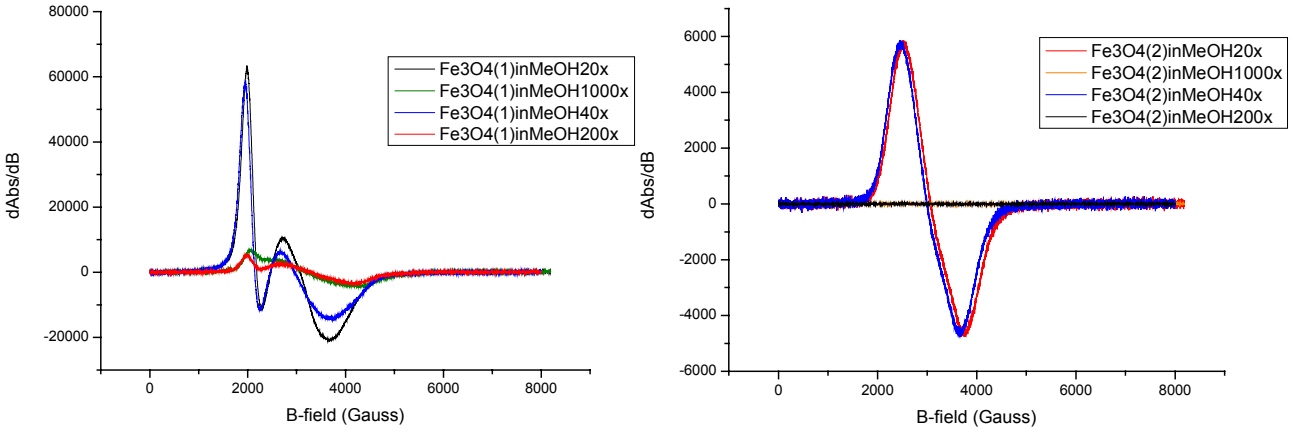

Figure 2.5: EPR spectrum of dilutions of magnetite nanoparticles in methanol
a) Fe_3O_4 with DEG and NMDEA on the surface;
b) Fe_3O_4 with DEG and DEA on the surface

Fe_3O_4 (DEG, NMDEA) in MeOH	X_{min}	X_{max}	ΔB	B_{eff}	ΔB_{low}	ΔB_{high}	A	g_{eff}
20X	1982.80	3675.27	1692.47	3060.21	1077.41	615.06	0.57	2.3
40X	1956.99	3675.27	1718.28	2952.69	995.70	722.58	0.72	2.3
200X	1993.55	4197.85	2204.30	3302.16	1308.61	895.69	0.68	2.1
200X	2073.12	4260.22	2187.10	3236.72	1163.60	1023.50	0.88	2.8
Fe_3O_4 (DEG, DEA) in MeOH	X_{min}	X_{max}	ΔB	B_{eff}	ΔB_{low}	ΔB_{high}	A	g_{eff}
20X	2521.19	3747.26	1226.07	3067.54	546.35	679.72	1.24	2.3
40X	2460.96	3654.76	1193.80	2994.41	533.45	660.35	1.24	2.4

Table 2.2: Parameters of magnetite nanoparticles EPR spectra of dilutions of magnetite nanoparticles in methanol;
a) Fe_3O_4 with DEG and NMDEA on the surface;
b) Fe_3O_4 with DEG and DEA on the surface

The lineshapes of the SPR spectra of dilutions of magnetite nanoparticles in methanol sharpened asymptotically around 2 mg/mL magnetite nanoparticles. Below this concentration, the SPR lineshapes remained unchanged and the solutions were deemed magnetically dilute.

2.3.2 Characterization of citric acid-magnetite nanoparticles bioconjugates using EPR spectroscopy

Solutions of the magnetite samples with DEG and NMDEA on the surface different concentrations of citric acid (0.25 mg/mL, 0.5 mg/mL, 1 mg/mL, 1.25 mg/mL, 1.5 mg/mL) in the ratio 9:1, Fe_3O_4 to citric acid in methanol, were prepared and used for the investigation of the citrate ligand influence on the SPR spectra. Three hours after preparing the capillary tubes with the Fe_3O_4 nanoparticles in methanol and citric acid at all concentrations, the magnetite nanoparticles precipitated on the bottom of the tubes. The presence of the citric acid causes the precipitation of the magnetite nanoparticles in solution. Acquired SPR spectra of the citric acid-magnetite nanoparticles solutions and their calculated parameters are showed below.

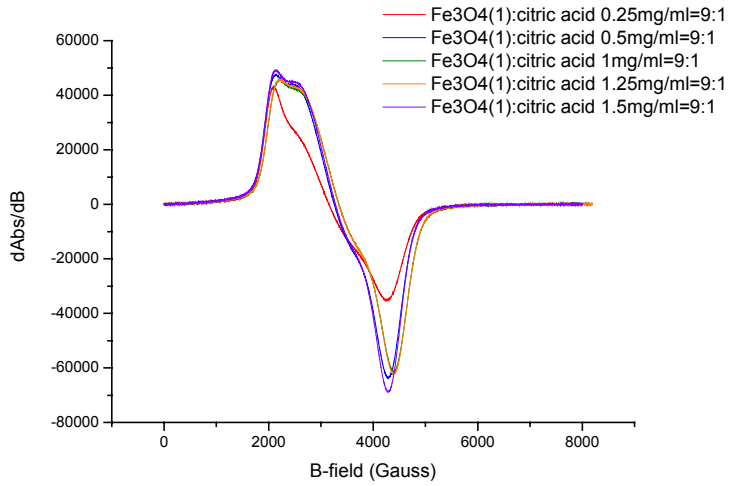

Figure 2.6: EPR spectrum of citric acid-magnetite nanoparticles solutions

Fe_3O_4-citric acid in MeOH	X_{min}	X_{max}	ΔB	B_{eff}	ΔB_{low}	ΔB_{high}	A	g_{eff}
0.25mg/mL	2093.14	4252.74	2159.60	3147.13	1053.99	1105.61	1.05	2.24
0.50mg/mL	2134.00	4276.41	2142.41	3254.68	1120.68	1021.73	0.91	2.16
1.00mg/mL	2198.54	4388.26	2189.72	3349.32	1150.78	1038.94	0.90	2.11
1.25mg/mL	2200.69	4383.96	2183.27	3338.57	1137.88	1045.39	0.92	2.11
1.50mg/mL	2129.71	4280.71	2151.00	3280.49	1150.78	1000.22	0.87	2.15

Table 2.3: Parameters of citric acid-magnetite nanoparticles EPR spectra

2.3.3 Characterization of salts-magnetite nanoparticles bioconjugates using EPR spectroscopy

The surface of magnetite nanoparticles has Fe^{2+} and Fe^{3+} ions with incomplete coordination spheres. The presence of ligands such as carbonate and acetate can complete the coordination of these ions [38]. To test this hypothesis, solutions of Fe_3O_4 nanoparticles with DEG and NMDEA on the surface in methanol (1 mg/mL) and acetate and respectively carbonate cosolutes (0.1 M) have been prepared and EPR signal of these salts-magnetite nanoparticles bioconjugates was collected (Figure 2.7).

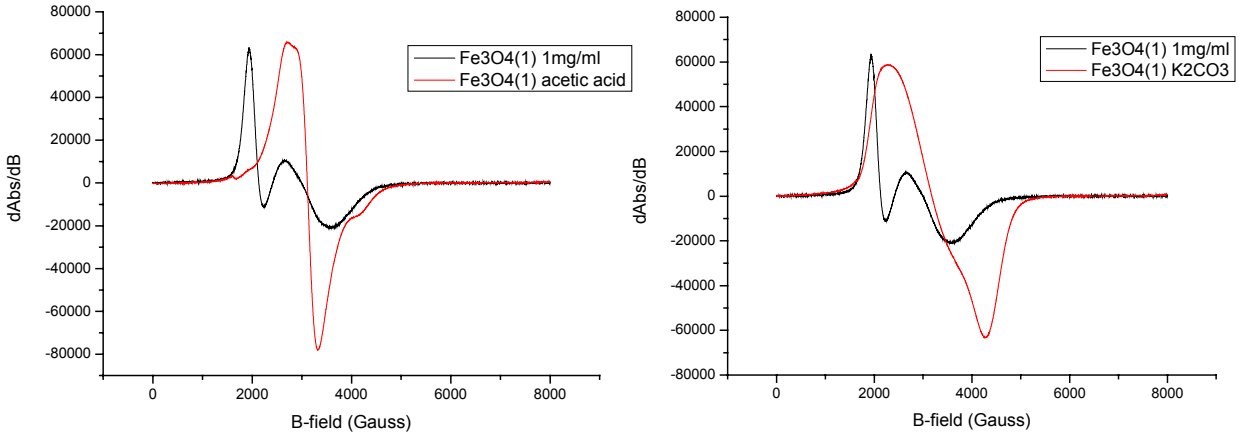

Figure 2.7: EPR spectra of salts-magnetite nanoparticles bioconjugates (compared with the EPR spectrum of magnetite nanoparticles)
a) Fe_3O_4 – acetic acid; b) Fe_3O_4 – potassium carbonate

The $g_{eff} \approx 4$ and $g_{eff} \approx 2$ transitions undergo important changes in the presence of the acetate and carbonate salts. The $g_{eff} \approx 4$ transition from distorted Fe^{3+} shifts to higher magnetic fields and/or merges with the $g_{eff} \approx 2$ super-paramagnetic iron-oxide resonances.

2.3.4 Characterization of proteins-magnetite nanoparticles bioconjugates using EPR spectroscopy

An alternative approach to complete the coordination of Fe^{2+} and Fe^{3+} ions on the surface of magnetite nanoparticles is to use proteins or polypeptides as ligands. The side-chains of proteins and polypeptides have carboxylates and amino groups that are able to form covalent-coordinative bonds with the Fe^{2+} and Fe^{3+} ions on the surface of the magnetite nanoparticles [39]. Bovine serum albumin (BSA) was used in this study. Although, BSA is a well-known stabilizer of the nanoparticles [21], the experiments proved that the magnetite nanoparticles with DEG and NMDEA on the surface aggregated after the addition of BSA. The EPR signal acquired from the precipitated nanoparticles is shown below.

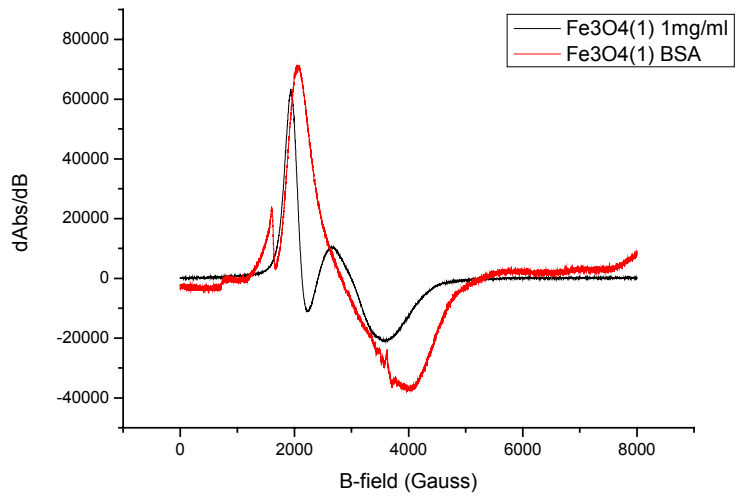

Figure 2.8: EPR spectrum of proteins (BSA)-magnetite nanoparticles bioconjugates (compared with the EPR spectrum of magnetite nanoparticles)

The resulting lineshape of the proteins (BSA)-magnetite nanoparticles bioconjugates EPR spectrum is intermediate of the acetate, and respectively carbonate, magnetite nanoparticles bioconjugates.

2.3.5 Characterization of magnetite nanoparticles in methanol solutions using EPR spectroscopy as a function of temperature

Both magnetite nanoparticles samples with DEG and NMDEA and respectively DEG and DEA on the surface, in methanol (2 mg/mL) were also studied by EPR at varying temperature. EPR data (Figures 2.9 and 2.10) were collected across a temperature range of 150-290 K and scaled to approximately the same peak intensity. The EPR signals of magnetite nanoparticles with DEG and NMDEA on the surface are dramatically different from the signals acquired from magnetite nanoparticles with DEG and DEA on the surface. The doublet at $g_{eff} \approx 3.59$ for magnetite nanoparticles with DEG and NMDEA on the surface is characteristic of Fe^{3+} in two states, labeled $Fe^{3+}_{(I)}$ and $Fe^{3+}_{(II)}$ [40]. The calculated EPR parameters, the dependence of linewidth, ΔB, with the changes of temperature, and the effective g-factor, g_{eff}, dependence on the temperature are also showed below.

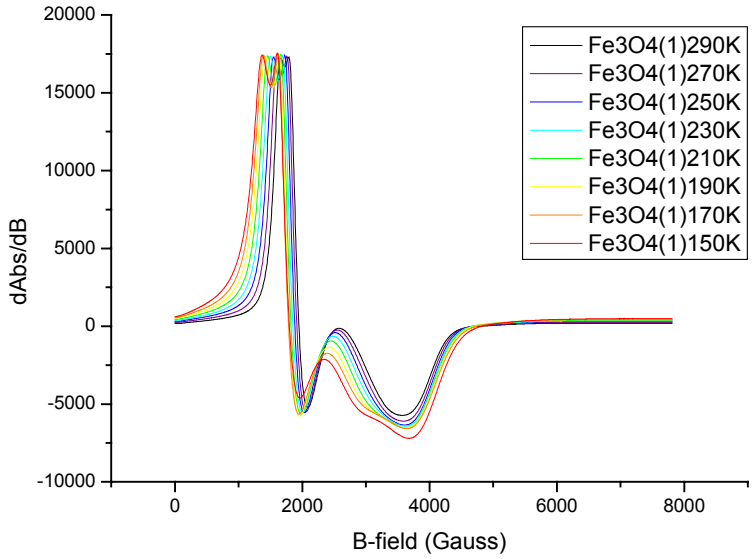

Figure 2.9: EPR spectra of magnetite nanoparticles in methanol as a function of temperature
Fe_3O_4 with DEG and NMDEA on the surface;

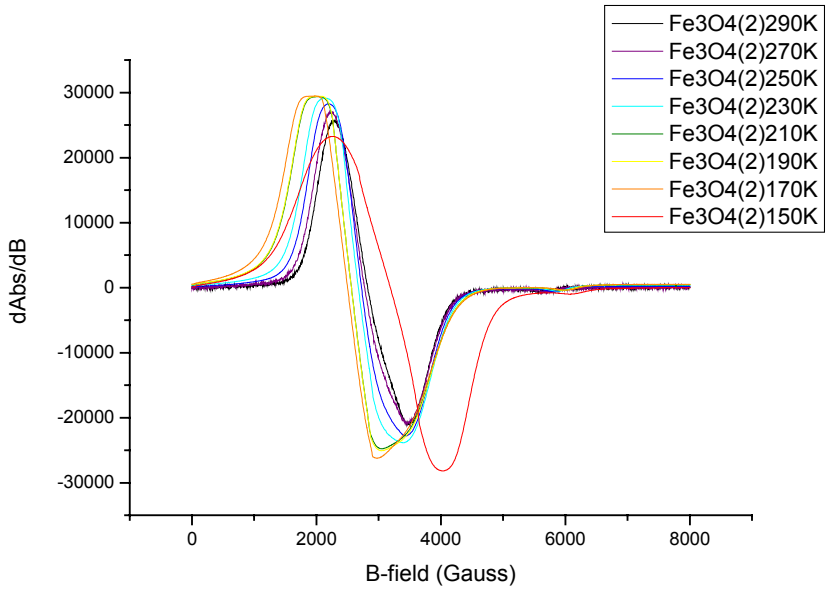

Figure 2.10: EPR spectra of magnetite nanoparticles in methanol as a function of temperature
Fe_3O_4 with DEG and DEA on the surface

Fe_3O_4 (DEG, NMDEA)	X_{min}	X_{max}	ΔB	B_{eff}	ΔB_{low}	ΔB_{high}	A	g_{eff}
290 K	1787.09	3578.49	1791.40	1950.54	163.45	1627.95	9.96	3.45
270 K	1759.14	3602.15	1843.01	1916.13	156.99	1686.02	10.73	3.51
250 K	1722.58	3619.35	1896.77	1883.87	161.29	1735.48	10.76	3.57
230 K	1690.32	3632.26	1941.94	1849.46	159.14	1782.80	11.20	3.63
210 K	1655.91	3640.86	1984.95	1821.51	165.60	1819.35	10.98	3.69
190 K	1634.41	3643.01	2008.60	1800.00	165.59	1843.01	11.13	3.74
170 K	1615.05	3647.31	2032.26	1782.79	167.74	1864.52	11.11	3.77
150 K	1610.75	3673.12	2062.37	1795.69	184.94	1877.43	10.15	3.75
Fe_3O_4 (DEG, DEA)	X_{min}	X_{max}	ΔB	B_{eff}	ΔB_{low}	ΔB_{high}	A	g_{eff}
290 K	2292.47	3498.92	1206.45	2821.50	529.03	677.42	1.28	2.38
270 K	2255.91	3455.91	1200.00	2774.19	518.28	681.72	1.32	2.42
250 K	2212.90	3451.61	1238.71	2724.73	511.83	726.88	1.42	2.47
230 K	2159.14	3384.95	1225.81	2675.27	516.13	709.68	1.37	2.51
210 K	2023.66	3053.76	1030.10	2563.44	539.78	490.32	0.91	2.62
190 K	2025.81	3043.01	1017.20	2561.29	535.48	481.72	0.90	2.63
170 K	1913.98	2967.74	1053.76	2498.92	584.94	468.82	0.80	2.70
150 K	2255.92	4025.81	1769.89	3187.09	931.17	838.72	0.90	2.11

Table 2.4: Parameters of magnetite nanoparticles EPR spectra as a function of temperature
a) Fe_3O_4 with DEG and NMDEA on the surface;
b) Fe_3O_4 with DEG and DEA on the surface

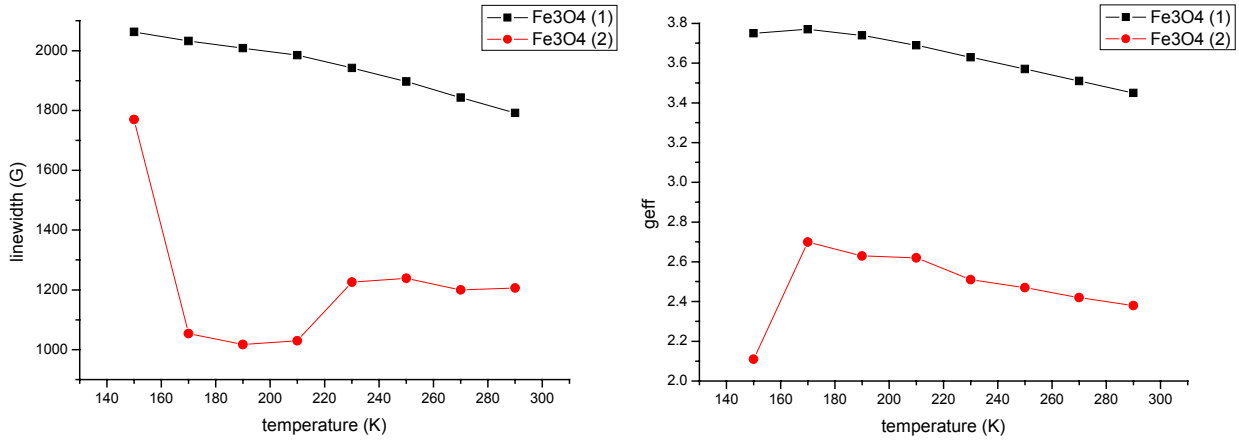

Figure 2.11: a) Linewidth, ΔB, dependence on the temperature;
b) Effective g-factor, g_{eff}, dependence on the temperature
1) Fe_3O_4 with DEG and NMDEA on the surface;
2) Fe_3O_4 with DEG and DEA on the surface

As the temperature decreases, there is a linear increase of the g_{eff}; below 170 K, the g_{eff} begins to decrease. The broad linewidth of the $g_{eff} \approx 2$ transition is characteristic of the superparamagnetic behavior of iron oxide compounds. The linewidth increases linearly as the temperature decreases and it displays the same deviations from linearity as g_{eff}.

2.3.6 Discussion

Although, TEM images show no differences between the two prepared magnetite nanoparticles samples (with DEG and NMDEA on the surface, and respectively, with DEG and DEA on the surface) [35], SPR spectra of these two samples look significantly different. For both samples, at concentrations below 2 mg/mL, dipolar exchange effects are minimal and magnetically dilute samples are obtained. The EPR signal became broader with the decrease of the magnetite concentration due to the changes in the interparticle interactions, so in spin-spin interactions.

Between 0.25 mg/mL and 0.5 mg/mL citric acid in methanol, saturation of the magnetite nanoparticles occurs. Citric acid is bound to the magnetite nanoparticles surface by a coordinative-covalent bond and it causes their precipitation at all concentrations. It is believed that citric acid changes the coating of the nanoparticles and causes agglomeration of the nanoparticles in solution [38]. Precipitation can also be caused by the destabilization of the magnetite electrostatic shell, similar to gold nanoparticle electrostatic shell (Figure 2.12). Although, this effect would produce the broadening of the EPR lines, the linewidth values for citric acid coated and uncoated magnetite nanoparticles are similar.

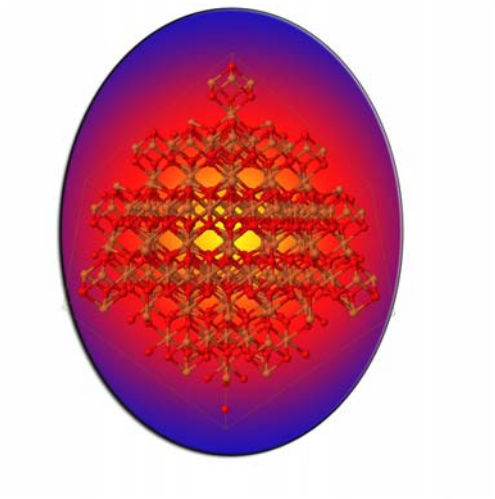

Figure 2.12: Magnetite nanoparticles electrostatic shell

EPR characterization of magnetite nanoparticles and different cosolutes solutions showed that precipitation of the nanoparticles occurs in the presence of cosolutes. The changes in the EPR spectra of magnetite nanoparticles with acetate and carbonate may be the result of the modification of the nanoparticles outer layer by these cosolutes (it is postulated that the outer layer of the magnetite nanoparticles with lower symmetry comparing to the interior gives the EPR spectrum [41]). At the surface of the nanoparticle

the coordination state of Fe^{3+}/Fe^{2+} ions is incomplete, so departures from axially symmetric states can occur. In the presence of ligands like acetate and carbonate salts, or proteins like BSA, these defects become minimal due to the binding that establish. The ligands bounded to the surface of the magnetite nanoparticles change the coordination environment of the Fe^{3+}/Fe^{2+} ions and they are responsible for the re-achievement of the axial symmetry of the Fe^{3+} ions. As a result of ligands linkage on the surface of the nanoparticles, the ferromagnetic behavior of the magnetite is altered.

g_{eff} and linewidths of the EPR spectra increase linearly with the decrease of the temperature for both magnetite nanoparticles samples. Also, at lower temperatures, the system being more ordered, there is less Brownian movement of the nanoparticles and the interactions are minimal, so the signal intensity decreases. As a consequence, the EPR line broadens and there is a shift of the signal down to lower fields. The linewidth values are almost linearly temperature dependent (Figure 2.11); as the temperature decreased, the linewidths increased, however, deviations from linearity begin to occur at 170 K.

The ferromagnetic transition takes place in magnetite at room temperature. At low temperature, the electron cannot move between Fe^{3+} and Fe^{2+} ions, this temperature being known as Verwey transition [42]. Below 125 K (the Verwey transition temperature, T_v), a change in the magnetite crystal structure also occurs. Above T_v, magnetite is cubic with a $Fe^{2.5+}$ charge resulting from the exchange between the two iron ions in octrahedral sites (Fe^{3+} and Fe^{2+}), while below T_v, magnetite has a monoclinic crystal structure with fixed charges. The g_{eff} and linewidths deviations from the linearity with temperature could reflect magnetite's impending Verwey transition. The phase transition from cubic to monoclinic is also responsible for these changes in the EPR spectra [43].

Single crystals of magnetite are known for having $g_{eff} \approx 2$ when the applied field is aligned with the nanoparticles easy axes. Due to the Brownian motion in the solution, in reality most of the nanoparticles easy axes are slightly differently oriented comparing to the direction of the applied magnetic field, so broad EPR signals and high g_{eff} values are obtained. With decreasing temperature, the probability of the nanoparticles to align their easy axis with the magnetic field is even lower, so more nanoparticles will be oriented off the direction of the magnetic field and this effect produces even a broader EPR signal [44]. At higher temperatures, Brownian motion favors the alignment of the nanoparticles easy axes with the applied magnetic field and a sharp EPR signal is obtained.

2.4 Conclusions

In summary, the initial hypothesis that ligands on the surface of the magnetite nanoparticles induce modifications in the characteristics of the SRP spectra was demonstrated. From the experiments it was concluded that the EPR signal is sensitive to the changes in the interparticle dipolar interaction upon dilutions. The $g_{eff} \approx 4$ transition from distorted Fe^{3+} is shifted to higher magnetic fields and the linewidths are increased by coatings on the surface of magnetite nanoparticles. EPR spectra of the magnetite nanoparticles are strongly dependent of temperature. The observed temperature dependence of the g_{eff} and linewidths is accounted for by the averaged thermal fluctuations of the magnetocrystalline anisotropy energy. Changes in the EPR spectra of the magnetite nanoparticles with ligands immobilized on the surface of the particles are an indication that these biomagnetic systems can be used further as sensors for detecting the conformational changes in a protein.

References

[1] Niemeyer, C. M., *Angew. Chem. Int. Ed.*, 2001, 40, 4128-4158;

[2] Zhang, S., *Nature Biotechnology*, vol. 21, 2003, 10, 1171-1178;

[3] Fitzmaurice, D.; Connolly, S., *Adv. Mater*., 1999, 11, 1202-1205;

[4] Manna, L.; Parak, W. J., *Small*, 2005, 1, 48-63;

[5] Mahtab, R.; Harden, H. H.; Murphy, C. J., *J. Am. Chem. Soc.*, 2000, 122, 14-17;

[6] Mattoussi, H.; Mauro, J. M.; Goldman, E. R.; Anderson, G. P.; Sundar, V. C.; Mikulec, F. V.; Bawendi, M. G., *J. Am. Chem. Soc.*, 2000, 122, 12142-12150;

[7] Chan, W. C.; Nie, S.; *Science*, 1998, 281, 2016-2018;

[8] Park, S. J.; Taton, T. A.; Mirkin, C. A., *Science*, 2002, 295, 1503-1506;

[9] Storhoff, J. J.; Elghanian, R.; Mucic, R. C.; Mirkin, C. A.; Letsinger, R. L., *J. Am. Chem. Soc.*, 1998, 120, 1959-1964;

[10] Hardman, R., *Environmental Health Perspective*, 2006, 114, 165-172;

[11] Berry, C.; Curtis, A. S., *J. Phys. D: Appl. Phys.*, 2003, 36, 198-206;

[12] Ito, A.; Tanaka, K.; Kondo, K.; Shinkai, M.; Honda, H.; Matsumoto, K.; Saida, T.; Kobayashi, T., *Cancer*, 2003, 94, 308-313;

[13] Zheng, M.; Huang X., *J. Am. Chem. Soc.*, 2004, 126, 12047-12054;

[14] Gray, J. J., *Current Opinion in Structural Biology*, 2004, 14, 110-115;

[15] Creighton, T. E., editor, *Protein Folding*, 2000, 17-25;

[16] Creighton, T. E., *Proteins*, 1993, 296-303;

[17] Shakhnovich, E., *Chem. Rev.*, 2006, 106, 1559-1588;

[18] Taubes, G., *Science*, 1996, 271, 1493-1495;

[19] Hayat, M. A., *Colloidal Gold Principles, Methods, and Applications*, 1989, vol.1, 1-3;

[20] Geoghegan, W. D.; Ackerman, G. A., *The Journal of Histochemistry and Cytochemistry*, 1977, 25, 1187-1200;

[21] Birrell, G. B.; Hedberg, K. K.; Griffith, O. H., *The Journal of Histochemistry and Cytochemistry*, 1987, 35, 843-853;

[22] Chah, S.; Hammond, M.; Zare, R. N., *Chemistry & Biology*, 2005, 12, 323-328;

[23] Economou, E. N., *Physical Review*, 1969, 182, 539-554;

[24] Neogi, A.; Morkoc, H., *Nanotechnology,* 2004, 15, 1252-1255;

[25] Nanogold – product information, Nanoprobes Inc., 2000;

[26] Chan, W. C.; White, P. D., *Fmoc Solid Phase Peptide Synthesis*, 2000, 65-71;

[27] Hase, S.; Ikenaka, T., *Anal. Biochem.*, 1090, 184, 135-138;

[28] Song, H. T.; Choi J.; Huh, Y. M.; Kim, S.; Jun Y.; Suh, J. S.; Cheon, J., *J. Am. Chem. Soc.*, 2005, 127, 9992-9993;

[29] Pankhurst, Q. A.; Connolly, J.; Jones, S. K.; Dobson, J., *J. Phys. D: Appl. Phys.*, 2003, 36, 167-181;

[30] Berger, R.; Kliava, J.; Bissey, J. C.; Baietto, V., *J. Phys. Condens. Matter,* 1998, 10, 8559-8572;

[31] Kliava, J.; Berger, R., *Journal of Magnetism and Magnetic Materials*, 1999, 205, 328-342;

[32] Berger, R.; Bissey J. C.; Kliava, J.; Daubric, H.; Estournes, C., *Journal of Magnetism and Magnetic Materials*, 2001, 234, 535-544;

[33] Weiss, B.; Kim, S. S.; Kirschvink, J. L.; Kopp, R. E.; Sankaran, M.; Kobayashi, A.; Komeili, A., *Earth and Planetary Science Letters*, 2004, 224, 73-89;

[34] Weiss, B.; Kim, S. S.; Kirschvink, J. L.; Kopp, R. E.; Sankaran, M.; Kobayashi, A.; Komeili, A., supplementary material, *Earth and Planetary Science Letters*, 2004, 224, 73-89;

[35] Caruntu, D.; Remond, Y.; Chou, N. H.; Jun, M. J.; Caruntu, G.; He, J.; Goloverda, G.; O'Connor, C. J.; Kolesnichenko, V., *Inorg. Chem.*, 2002, 41, 6137;

[36] Berger, P., *J. Chem. Ed.*, 1999, 76, 943-948;

[37] Cox, P. A, *The Electronic Structure and Chemistry of Solids*, 1991, 157-160;

[38] Sharma, V. K.; Waldner, F., *Journal of Applied Physics*, 1977, 48, 4298-4302;

[39] Koseoglu, Y.; Yildiz, F.; Kim, D. K.; Muhammed, M.; Aktas, B., *Phys. Stat. Sol. C*, 2004, 12, 3511-3515;

[40] Angel, B. R; Vincent, W. E. J., *Clays and Clay Minerals*, 1978, 26, 263-272;

[41] Mikhaylova, M.; Kim, K.; Bobrysheva, M.; Osmolowsky, M.; Semenov, V.; Tsakalakos, T.; Muhammed, M, *Langmuir*, 2004, 20, 2472-2477;

[42] Koksharov, Y. A., *Journal of Applied Physics*, 2001, 89, 2293-2298;

[43] Koseoglu, Y.; Aktas, B., *Phys. Stat. Sol. C*, 2004, 12, 3516-3520;

[44] Berger, R.; Bissey, J. C.; Kliava, J., *J. Phys. Condens. Matter*, 2000, 12, 9347-9360.

Vita

Larisa Cristina Radu was born in Tecuci, Romania. In 2003, she got her BS degree in Biomedical Engineering from “Gr. T. Popa” University of Medicine and Pharmacy, Iasi, Romania. In 2004, she enrolled in the chemistry graduate program at University of New Orleans, and same year, she joined Dr. John B. Wiley solid state and nanomaterials research group.